Environmental Science & Technology

Article

Cite This: Environ. Sci. Technol. XXXX, XXX, XXX−XXX

pubs.acs.org/est

Catalytic Hydrogel Membrane Reactor for Treatment of Aqueous Contaminants

Randal Marks,[†] Joseph Seaman,[‡] Patricia Perez-Calleja,[†] Junyeol Kim,[†] Robert Nerenberg,[†] and Kyle Doudrick*[,†]

[†]University of Notre Dame, Department of Civil and Environmental Engineering and Earth Sciences Notre Dame, Indiana, 46556 United States

[‡]University of Notre Dame, Department of Chemical and Biomolecular Engineering Notre Dame, Indiana, 46556 United States

Supporting Information

ABSTRACT: Heterogeneous hydrogenation catalysis is a promising approach for treating oxidized contaminants in drinking water, but scale-up has been limited by the challenge of immobilization of the catalyst while maintaining efficient mass transport and reaction kinetics. We describe a new process that addresses this issue: the catalytic hydrogel membrane (CHM) reactor. The CHM consists of a gas-permeable hollow-fiber membrane coated with an alginate-based hydrogel containing catalyst nanoparticles. The CHM benefits from counter-diffusional transport within the hydrogel, where H_2 diffuses from the interior of the membrane and contaminant species (e.g., NO_2^-, O_2) diffuse from the bulk aqueous solution. The reduction of O_2 and NO_2^- were investigated using CHMs with varying palladium catalyst densities, and mass transport of reactive species in the catalytic hydrogel was characterized using microsensors. The thickness of the "reactive zone" within the hydrogel affected the reaction rate and byproduct selectivity, and it was dependent on catalyst density. In a continuously mixed flow reactor test using groundwater, the CHM activity was stable for a 3 day period. Outcomes of this study illustrate the potential of the CHM as a scalable process in the treatment of aqueous contaminants.

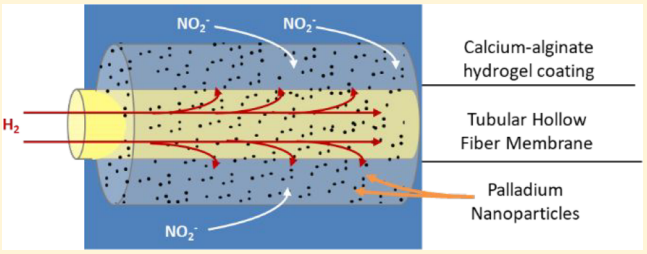

INTRODUCTION

Heterogeneous hydrogenation catalysis (HHC) is a promising advanced reduction process for the treatment of oxidized contaminants using hydrogen gas (H_2).[1−6] For water treatment applications, target reactions occur at the interface between solid (catalyst), liquid (water), and gas (H_2) phases. Palladium (Pd) is the most widely studied catalyst for HHC due to high activity and desirable selectivity.[7,8] While attempts have been made to replace Pd and other platinum group metals (PGMs) with more earth-abundant materials (e.g., metals sulfides and phosphides), their activities are orders of magnitude lower than PGMs,[9] they are unstable in aqueous environments,[10] and/or they require high operating pressures and temperatures.[11] Thus, PGMs still remain the optimal choice,[12] and though they are costly, recent advances in nanotechnology have made PGM catalysts cost competitive compared to other treatment technologies (e.g., ion exchange, air stripping, activated carbon adsorption).[13−16] To date, full-scale HHC implementation has yet to come to fruition due to challenges including mass transfer limitations, costs, catalyst instability, and scalability of current treatment options.

Conventional slurry reactors use catalysts that are supported on an inorganic substrate, e.g., activated carbon, alumina, or silica. These supported catalysts are suspended in the aqueous phase, and H_2 is bubbled directly into the aqueous phase.[17] While simple to operate, this approach suffers from the disintegration of powdered catalysts due to particle abrasion during mixing, post filtration requirements, inefficient H_2 consumption, and/or H_2 safety concerns.[4] Using fixed (or packed) bed catalytic reactors alleviates the need for both rapid stirring of the catalyst solution and post-treatment filtration.[4,7] For example, the trickle-bed reactor is effective for treating aqueous nitrate,[13,16,18−21] but it has limited reactivity due to H_2 solubility limits and poor mass transfer to catalyst surface as well as biofilm fouling during long-term operation.[19] Reactors that use highly structured immobilized catalyst supports (e.g., monoliths,[22−24] cloth,[25−29] foam,[30,31] and forced-flow membranes[32,33]) can address mass transfer limitations on reactivity caused by large particle sizes used in traditional packed bed reactors.[18,25,34]

Three-dimensional interfacial catalytic membranes are an exciting approach to immobilized catalyst reactors that allow for a dense loading of nanosized catalysts and deliver H_2 through a counter-diffusional pathway. In a typical interfacial membrane reactor configuration, catalyst particles are loaded onto the surface of a gas- or aqueous-permeable membrane. Gaseous and aqueous phases are introduced on opposite faces

Received: March 18, 2019
Revised: May 12, 2019
Accepted: May 14, 2019
Published: May 14, 2019

DOI: 10.1021/acs.est.9b01667
Environ. Sci. Technol. XXXX, XXX, XXX−XXX

of the membrane and interact as gas diffuses through the membrane toward the catalyst. This configuration enables independent control of aqueous and gaseous operating conditions, which allows for improved control of the reaction, operational safety, and H_2-consumption efficiency compared to systems based on H_2 bubbling into the aqueous phase.[35,36] In membrane biofilm reactors, the gas-transfer efficiency has been shown to approach 100%.[37−40] Membrane-type reactors have previously been demonstrated for hydrogenation reactions using alumina tubular membranes loaded with catalyst particles for NO_2^- reduction; ammonia selectivity was controlled through modification of H_2 partial pressure within the reactor.[36,41−43] However, such reactors suffer from complex catalyst synthesis procedures, poor control of catalyst loading, and low contaminant reaction rates. New types of catalyst support are needed to address these challenges.

In this study, a novel type of HHC architecture was developed and characterized: the catalytic hydrogel membrane (CHM) reactor. The CHM consists of a gas-permeable hollow-fiber membrane (HFM) coated with an alginate-based hydrogel that contains catalyst nanoparticles. The CHM operates by using counter-diffusional transport of reactive species within the hydrogel, where H_2 diffuses from the interior of the membrane and dissolved target species (e.g., dissolved oxygen) diffuse from the bulk aqueous solution. Counter-diffusional delivery of H_2 reduces consumption of H_2 and allows the reaction to be "tuned" toward desired byproducts. The CHM reactor is the first to use hydrogels for catalyst immobilization in conjunction with counter-diffusional membrane techniques. Herein, the CHM concept is developed with a model catalyst (Pd) and model contaminants (O_2 and NO_2^-). Specifically, this study (i) develops and physically characterizes a CHM with Pd nanoparticle catalysts, (ii) investigates the counter-diffusional behavior of the CHM using O_2 as a model contaminant, (iii) provides a proof-of-concept study assessing the reduction of a water contaminant, NO_2^-, as a function of Pd loading, (iv) demonstrates the effects of H_2 delivery mode and mass transport limitations on the activity and byproduct selectivity of NO_2^- reduction, and (v) establishes the short-term stability of the CHM reactor for reduction of NO_2^- over a 3 day period.

MATERIALS AND METHODS

2.1. Assembly of the Catalytic Hydrogel Membrane. The CHM consists of a gas-transfer HFM coated with a calcium-alginate hydrogel that is embedded with catalytic nanoparticles (Figure 1). The Ca-alginate hydrogel was selected as a catalyst matrix due to its low cost, simple synthesis process, and desirable properties in aqueous solution. Alginate hydrogels have been reported as effective matrices for catalytic metal nanoparticles including gold,[44,45] silver,[46−48] platinum,[49] and palladium.[50] Ca-alginate hydrogels form when the guluronate regions of the alginate biopolymer cross-link with Ca^{2+} ions to form a three-dimensional structure.[51] The cross-linked characteristic of the polymer allows for effective immobilization of catalyst nanoparticles within the alginate matrix. Further, the highly aqueous nature of the hydrogel provides limited resistance to the transport of dissolved species, e.g., H_2, O_2, and NO_2^-.[52]

The CHM was constructed using a novel method involving the in situ reduction of Pd^{2+} ions enmeshed in a Ca-alginate hydrogel. Briefly, 2% (m/m) alginic acid sodium salt (low viscosity, #01469, Chem-Implex Inc.) was dissolved in ultrapure water (18.2 MΩ-cm) with stirring until homogeneity was achieved. The alginate solution was transferred to a custom-built half-tube reactor for coating. A 25 cm length of the silicone HFM (0.037" o.d. × 0.025" i.d., #025BRA002, Braintree Scientific, Saint Gobain) was completely submerged in the alginate solution. A 20 mL cross-linking solution (100 mM total concentration) was prepared by dissolving calcium chloride ($CaCl_2$, anhydrous, #C77, Fisher Scientific) and palladium nitrate dihydrate ($Pd(NO_3)_2 \cdot 2H_2O$, #76070, Sigma-Aldrich) in aqueous solution, which was then poured into a separate half-tube reactor. The alginate-coated membrane was removed from the alginate solution and rapidly transferred to the Ca^{2+}/Pd^{2+} cross-linking solution. The membrane was soaked in the cross-linking solution for 30 min to allow for complete cross-linking. The resulting Ca-alginate hydrogel had a vibrant orange color from Pd^{2+} intrusion. The alginate coating and cross-link procedure was repeated once to increase the hydrogel thickness and stability. Finally, the reduction of the embedded Pd^{2+} to Pd nanoparticles was induced by submerging the membranes in 2.5 mM sodium borohydride ($NaBH_4$, 98%, #13432, Alfa-Aesar), during which the hydrogel turned a dark gray color. The completed catalytic hydrogel membrane was stored in ultrapure water until use.

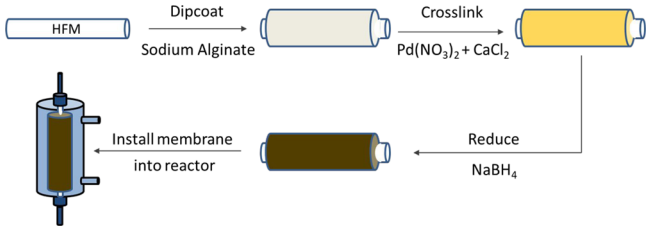

Figure 1. Growth process for catalytic hydrogel film on an HFM. A clean HFM is dipped in an aqueous solution of sodium alginate and then rapidly transferred to a solution of $Pd(NO_3)_2$ and $CaCl_2$ to cross-link. After cross-linking is complete, Pd^{2+} ions are reduced in a sodium borohydride solution to form Pd nanoparticles. The coated membrane is then installed in a glass reactor for hydrogenation catalysis experiments.

2.2. Hydrogenation of NO_2^-. To conduct the NO_2^- hydrogenation experiments, the CHM was installed in a tubular glass reactor with ports for aqueous and gaseous supplies, which formed the CHM reactor assembly (Figure S1). The aqueous solution was composed of ultrapure water (18.2 MΩ-cm) and 0.35 mM of sodium nitrite ($NaNO_2$, reagent grade, #0535, VWR). For all counter-diffusional experiments, 100% H_2 (ultrahigh purity, #HY UHPT, American Gas and Welding) was supplied through the lumen of the HFM (operated in closed mode, constant lumen pressure of 3 psi). The majority of experiments were conducted in a recirculating batch system, where the aqueous solution (volume = 60 mL) was recycled along the exterior of the CHM using a peristaltic pump. A single experiment using groundwater was conducted using a completely mixed flow reactor consisting of eight CHMs bundled. This reactor setup and the groundwater characterization are described in more detail in the SI (Figure S2, Table S1). During hydrogenation experiments, bulk aqueous aliquots were removed periodically for subsequent analysis of NO_2^- and NH_4^+ by ion chromatography (IC; Dionex ICS 5000+; AS-23 and CS-12A analytical columns). The sole byproducts were assumed to be

DOI: 10.1021/acs.est.9b01667
Environ. Sci. Technol. XXXX, XXX, XXX−XXX

N_2 and NH_4^+, so N_2 formation was calculated from the mass balance between measured NO_2^- and formed NH_4^+.

2.3. Materials Characterization of the CHM. Optical coherence tomography (OCT; Ganymede II Spectral Domain OCT System, THORLABS, Inc.) was used to obtain optical 2D sections of the internal structure of the catalytic hydrogel while it was submerged in ultrapure water. Pd nanoparticles were extracted from the hydrogel by dissolving it in a solution of ethylenediaminetetraacetic acid (0.1 M) and sodium citrate (0.2 M). The isolated particles were then centrifugally washed and resuspended in ethanol. A drop of this solution was added to a transmission electron microscopy (TEM) grid, dried, and then analyzed by TEM (Titan 80−300, 300 kV) to obtain the primary particle size. The Pd crystal structure was characterized using selected area electron diffraction (SAED). The total Pd mass loading in each CHM was determined using inductively coupled plasma-optical emission spectroscopy (ICP-OES; PerkinElmer Optima 8000). To prepare the samples for ICP-OES, the hydrogel was first stripped from the HFM, dried in air at room temperature overnight, massed, and then digested in concentrated nitric acid (68%, redistilled, GFS) using microwave digestion (210 °C for 45 min, 110 mL MarsXpress vessel, Mars 6 Microwave Digester).

2.4. Microsensor Analysis of Concentration Profiles. To measure the concentration profiles of dissolved species O_2 and H_2 during catalytic O_2 reduction, a single-coated CHM was installed in a custom-built tubular glass reactor (6 mm inner diameter and 25 cm length) containing two ports for microsensor measurements (Figure S3). During operation, 100% H_2 (ultrahigh purity, #HY UHPT, American Gas and Welding) was supplied through the lumen of the HFM (open mode, 1 psi), while 100% O_2 (ultrahigh purity, #OX UHPT, American Gas and Welding) was constantly bubbled into the aqueous reservoir to achieve a high dissolved O_2 concentration. The aqueous solution was recycled through the reactor at a flow velocity of 2.7 cm s^{-1}. Prior to analysis, the system was operated for 0.5 h to obtain steady-state conditions. As a control, in separate experiments, 100% N_2 (high purity, #NI-300-HP, American Gas and Welding) was bubbled either into the lumen or the aqueous solution to analyze the absence of a reductant gas.

H_2 and O_2 microscale electrodes, or microsensors, with a 25 μm tip diameter (H2-25 and OX-25, Unisense A/S, Denmark) were used to measure the dissolved H_2 and O_2 profiles within the catalytic hydrogel. Microsensors were calibrated according to manufacturer's instructions, and data was collected using Unisense Logger 2.7 software. The microsensors, controlled with a motorized micromanipulator (model MC-232 and MM33, Unisense A/S), were inserted into the catalytic hydrogel perpendicular to the membrane until contact was established with the outer wall of the HFM. Measurements of species concentrations were then taken at 20 μm intervals as the microsensors were withdrawn through the hydrogel. Measurements were continued for another 400 μm into the bulk aqueous layer. The total measurement time for each profile was approximately 5 min.

RESULTS AND DISCUSSION

3.1. Material Characterization of the CHM. As observed in the TEM micrographs (Figure 2A), the average primary particle size of the Pd particles was 4.59 ± 1.02 nm (Figure 2B). SAED analysis revealed the presence of numerous Pd facets, including [111], [200], [220], [311], and [300] (Figure S4). Using the TEM micrographs, an average *d*-spacing of 0.23 nm was measured, which matches the [111] crystal facet for Pd and indicates it is the dominate facet.

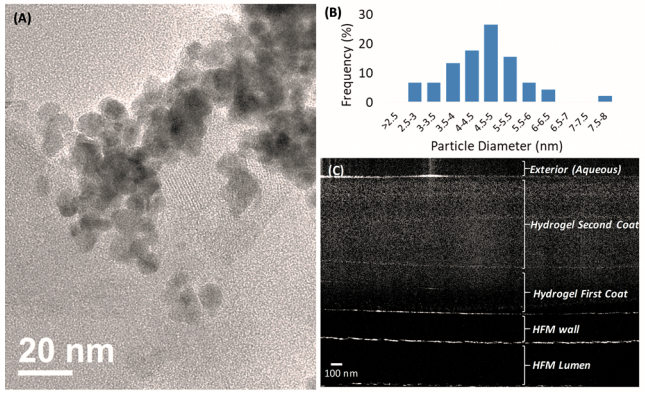

Figure 2. (A) TEM image of Pd nanoparticles isolated from hydrogel support. (B) Histogram of particle diameters measured from TEM images showing a normal distribution. (C) OCT cross-sectional image of hydrogel on HFM. The lower two white lines delineate the HFM wall, with the hydrogel above.

The color of the hydrogel of the CHM was dark gray and consistent throughout with no visible particles or aggregates. OCT images (Figure 2C) confirmed uniform dispersion of the Pd particles as no large aggregates were observed, and they showed that the mean thicknesses of the hydrogel for a single-layer and double-layer coated HFM were 304 ± 37 μm and 988 ± 119 μm, respectively. Longitudinal uniformity of Pd was investigated by analyzing the Pd-loading for 10 equiv 2.5 cm segments of a single CHM. The Pd-loading was found to be consistent with an average Pd mass of 0.184 ± 0.021 mg for one segment. With regards to the hydrogel film stability (i.e., adherence to the HFM and consistency within the gel), Pd-loadings greater than a theoretical Pd wt/dry alginate wt of 12.5% resulted in stability loss for the alginate viscosity/concentration used herein. The stability loss was presumably due to the decrease of alginate cross-linking sites as Pd^{2+} was reduced to Pd^0. Consequently, 12.5% theoretical Pd wt/ dry alginate wt was the maximum loading used in this study.

3.2. Microsensor Analysis of H_2 and O_2 transport through the CHM. To investigate the effects of counter-diffusional delivery of H_2 and the reactant on CHM behavior, microsensor analysis was used to map the concentration profiles of relevant species during hydrogenation. CHMs provide a unique opportunity for the direct observation of concentration profiles within the catalyst support. These profiles have been proposed previously for similar inorganic membrane supports, but they have not been quantified.[41,42] Microsensors have been established in the field of biofilms for the assessment of concentration profiles within the films, and they can be simply applied to the CHM due to the similar structural characteristics of the biofilm and alginate hydrogel.[53] Pd is known to catalyze the reduction of O_2 in the presence of H_2;[54] it was used as a model reaction because the reactants can be measured by commercially available microsensors and steady-state conditions of the reaction are easily maintained within the CHM.

The concentration profiles of O_2 and H_2 in a CHM as measured by the microsensor are shown in Figure 3. These profiles illustrate the concentrations of each species through the depth of the hydrogel and into the bulk aqueous zone.

DOI: 10.1021/acs.est.9b01667
Environ. Sci. Technol. XXXX, XXX, XXX−XXX

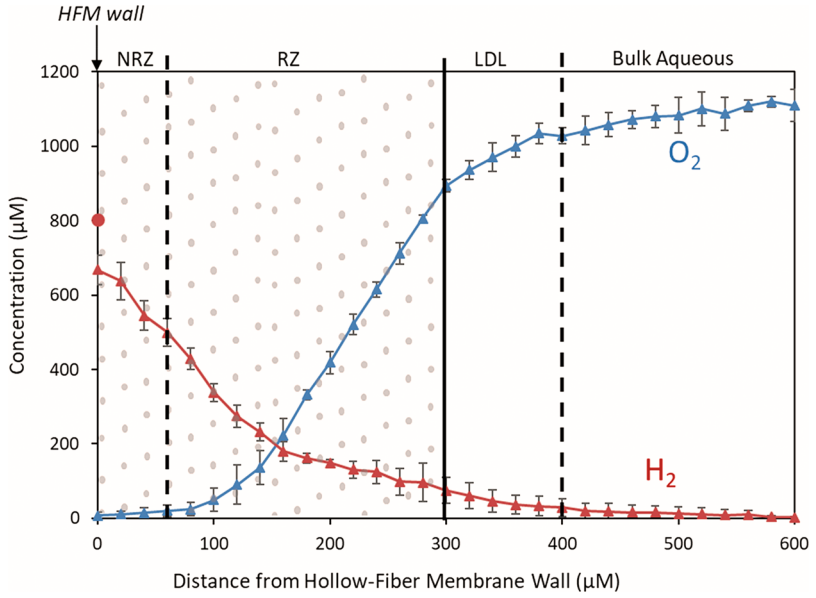

Figure 3. Concentration profiles of O_2 and H_2 during catalytic reduction of O_2 by a CHM as measured by microsensors. H_2 diffuses out of the HFM wall (left) and through the hydrogel (dotted region), while O_2 passes from the aqueous region (right) through the hydrogel. Reaction of H_2 and O_2 at catalytic sites results in the formation of distinct regions given at top of figure. NRZ: nonreactive zone, RZ: reactive zone, LDL: liquid diffusion layer. Dashed lines indicate estimated transition points between these regions, and the solid line indicates the outer edge of catalytic hydrogel. The red dot at the HFM wall represents the saturation concentration of H_2 at room temperature, which is not achieved in the system due to mass transfer limitations on H_2 diffusion through the HFM wall.

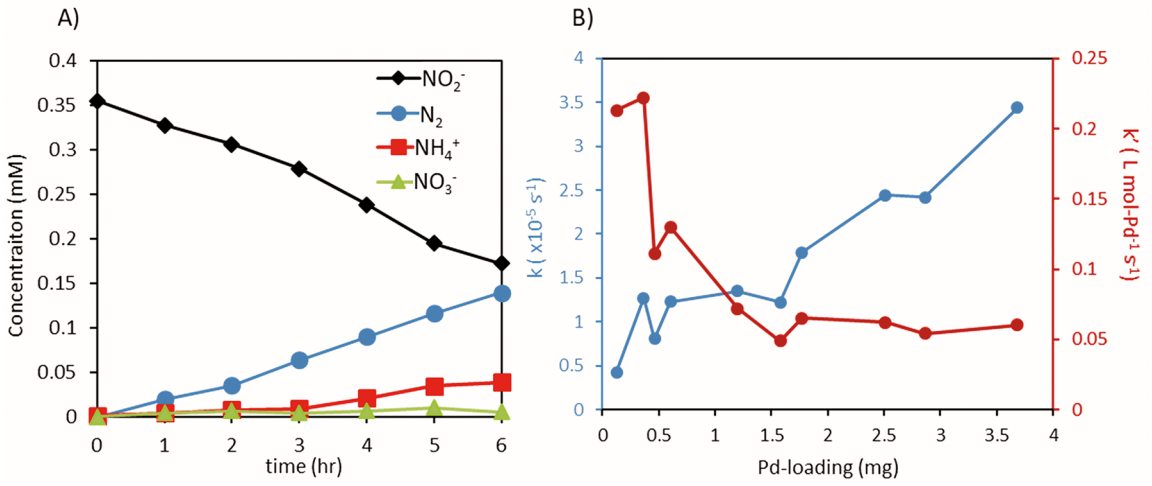

Figure 4. (A) Kinetics of NO_2^- removal by a CHM containing 3.68 mg of Pd. (B) Rate constants of NO_2^- removal as a function of total Pd embedded in the CHM; k' (blue) is the observed rate constant, and k (ed) is the Pd mass-normalized rate constant.

Distinct regions within the reactor were observed: the bulk aqueous region, the liquid diffusion layer (LDL), the reactive zone (RZ) of the hydrogel, and the nonreactive zone (NRZ) of the hydrogel. This bulk aqueous region is dominated by the flow of water parallel to the membrane and maintains a high oxygen concentration due to rapid recirculation of oxygenated water (e.g., 2.7 cm s^{-1}) from the reservoir, while the bulk H_2 concentrations approached zero. At the LDL, i.e., the interface between the hydrogel and the bulk aqueous region where diffusion is the dominant mechanism of mass transfer, aqueous species concentrations vary in a linear fashion per Fick's first law of diffusion. The position of the inner edge of the LDL was determined through visual observation of the microsensor exiting the hydrogel, while the outer edge was determined empirically by evaluation of the position of the change in slope of the O_2 concentration gradient. LDL thickness was found to be approximately 100 μm under the tested conditions. After diffusion through the LDL, O_2 reaches the hydrogel surface. The exterior region of the hydrogel closest to the LDL is the RZ, where H_2 and O_2 are reacting at catalyst sites. In this region, component concentration profiles follow a typical diffusion-reaction shape as transport is controlled by both diffusion and catalyst-surface reaction rates. Finally, the interior region of the hydrogel closest to the HFM is the NRZ, where O_2 has been depleted and no further reaction is occurring. In this region, H_2 transport from the membrane wall is dominated by diffusion. Note that the locations of the RZ and NRZ vary depending on the H_2 and O_2 concentrations at the hydrogel boundaries, the catalyst density and activity, and the overall hydrogel thickness.

DOI: 10.1021/acs.est.9b01667
Environ. Sci. Technol. XXXX, XXX, XXX−XXX

The transport of H_2 and O_2 was further investigated by measuring their respective profiles with separate replacement of H_2 or O_2 with N_2, allowing their transport to be governed by diffusion only (Figure S5). According to conservation of flux, diffusivity of a species within the hydrogel can be determined from the difference in the concentration gradient between the hydrogel and the LDL (Table S2). The measured concentration gradients were used to determine effective diffusivities of O_2 and H_2 in the CHM, which were 6.2×10^{-6} and 11.0×10^{-6} cm^2 s^{-1}, respectively. These effective diffusivities are approximately 25% of their aqueous diffusivities, indicating that the alginate matrix does hinder diffusion. The diffusivity of dissolved O_2 in the CHM is greater than those reported for other common supports, such as alumina (3.2×10^{-6} cm^2 s^{-1})[42] and activated carbon (0.58×10^{-6} cm^2 s^{-1}).[55] The effective diffusivity within the CHM could potentially be improved by changing the alginate properties (e.g., viscosity, density), although changes to alginate integrity due to these properties will require further consideration in future studies.

3.3. Proof of Concept: NO_2^- Hydrogenation. The hydrogenation of NO_2^- under batch recirculating conditions was investigated for a 6 h period using a single CHM containing 3.68 mg of Pd (Figure 4A). Catalytic hydrogenation of NO_2^- over noble metal catalysts is a well-studied reaction and can reduce aqueous NO_2^- under atmospheric conditions.[22,36,56,57] NO_2^- reduction, a multistep process, leads to the formation of either N_2 or NH_4^+ as the primary byproducts.[58] Using the CHM, approximately 52% of the NO_2^- was reduced during the reaction period. Only a trace amount of nitrate (<0.01 mM) was observed, which was attributed to impurities in the NO_2^- stock solution because it was also present in the control samples. NO_2^- reduction was not observed in the absence of either H_2 or Pd.

The loading of Pd (i.e., density) within the hydrogel is a critical parameter that affects the reactivity of the CHM. An increase in the catalyst density should increase the number of active sites per hydrogel unit volume, thereby improving the overall reaction activity. To test this hypothesis, the percentage of NO_2^- converted, the observed pseudo first-order rate constant (k), and the mole-Pd normalized rate constant (k') were evaluated as a function of the Pd-loading (Table 1, Figure 4B). For expensive noble metal catalysts, normalizing the activity to the catalyst mass provides a better appreciation of the mass−cost relationship; thus, herein, the rate constant was normalized to moles of Pd per volume (i.e., k'). The Pd-loading in a single CHM was varied from 0.128 to 3.68 mg, corresponding to theoretical Pd wt/dry alginate wt loadings of 0.5% to 12.5%. The homogeneity of the Pd-loading was assumed to be consistent across samples.

The k for NO_2^- increased with Pd-loading (R^2 = 0.91), reaching a maximum of 3.44×10^{-5} s^{-1} for highest Pd mass used (Figure 4B). The opposite trend was observed for k'. A maximum of 0.213 L mol-Pd^{-1} s^{-1} was achieved at the lowest Pd-loading, and it decreased with increasing Pd-loading until leveling at loadings greater than 1.5 mg Pd. These trends, previously observed in similar studies,[27,59] suggest that an increase in the amount of Pd increases the overall removal rates at the expense of lowered catalytic efficiency per mass of Pd. For the CHM, this behavior can be best described by a relationship between the RZ thickness and the Pd-loading density, as conceptualized in Figure 5.

Table 1. Kinetics of NO_2^- Removal and Ammonia Selectivity for CHMs Containing Increasing Pd-Loadings[a]

Pd-Loading (mg)	Conversion (%)	k ($\times 10^{-5}$ s^{-1})	k' (L mol-Pd^{-1} s^{-1})	Ammonia Selectivity (%)
0.128	8.82	0.428	0.213	47.2
0.365	24.2	1.27	0.222	53.0
0.462	15.0	0.805	0.111	45.7
0.603	23.7	1.23	0.130	41.8
1.20	25.3	1.35	0.072	32.2
1.58	24.2	1.22	0.049	62.7
1.77	35.0	1.79	0.065	42.0
2.51	40.7	2.44	0.062	19.1
2.86	40.6	2.42	0.054	12.6
3.68	51.5	3.44	0.060	9.89

[a]First-order rate constants are given in normal units and with normalization for Pd mass. Reaction time was 6 h.

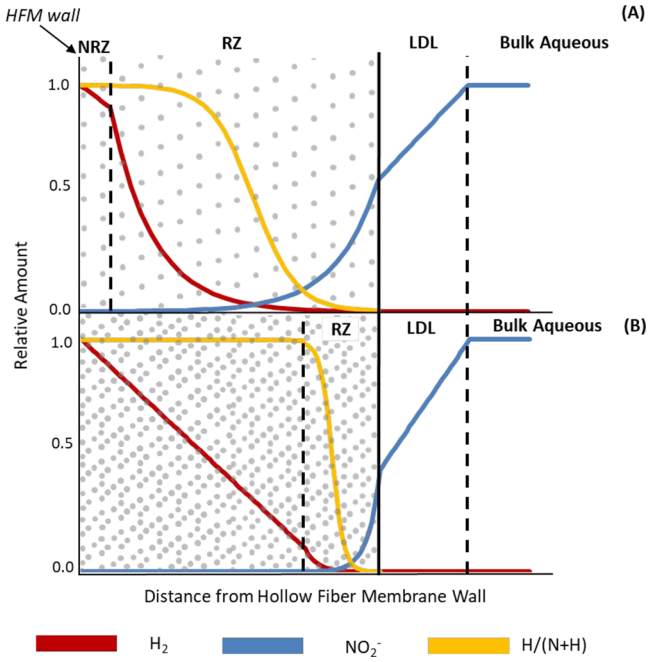

Figure 5. Conceptual diagram of counter-diffusional H_2 and NO_2^- transport in a CHM with (A) a low Pd-loading density and (B) a high Pd-loading density. The ratio of H_2 to N_2 throughout the hydrogel region is shown as a ratio of H_2 to the total H_2 + NO_2^- (yellow line). Note that H_2 and NO_2^- are relative amounts, i.e., concentrations divided by their highest concentration at the hydrogel boundary. Thus, they vary from 0 to 1. Shifts in RZ thickness are exaggerated for clarity.

At lower Pd-loadings, NO_2^- can diffuse deeper into the hydrogel from the bulk solution due to the lower density of available Pd sites. The result is a larger RZ within the hydrogel (Figure 5A), which will impart greater mass transfer limitations due to longer diffusion lengths. The larger RZ reduces k, but the Pd-mole normalized rate (k') benefits because more Pd throughout the hydrogel is utilized. Conversely, for higher Pd-loadings, there is a higher probability that NO_2^- will react with Pd-sites near the bulk aqueous solution without diffusing deeper into the hydrogel, creating a smaller RZ within the hydrogel (Figure 5B). The smaller RZ results in a faster k because internal diffusion effects are minimized, but it reduces the Pd mole-normalized rate (k') since less Pd is being used within the hydrogel (i.e., only Pd near the bulk solution).

DOI: 10.1021/acs.est.9b01667
Environ. Sci. Technol. XXXX, XXX, XXX−XXX

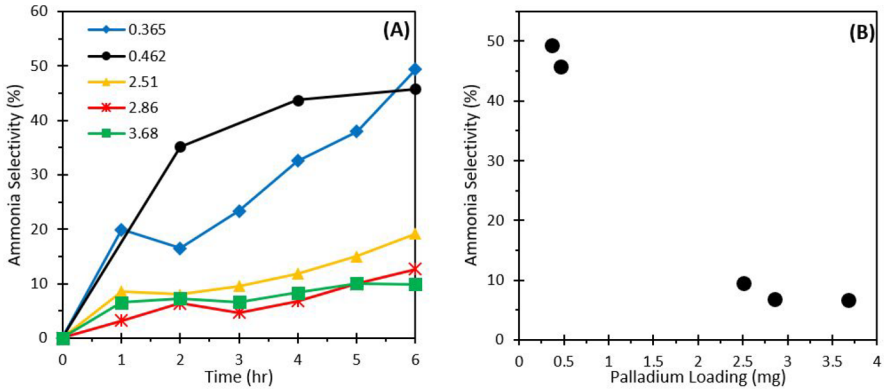

Figure 6. (A) NH_4^+ selectivity as a function of reaction time for CHMs with varying Pd-loadings. The Pd mass (mg) for each sample is given in the legend. (B) NH_4^+ selectivity as a function of Pd-loading for each sample at approximately 25% NO_2^- conversion.

Because diffusion within the hydrogel is progressively irrelevant with increasing Pd-loadings, k' eventually levels off and becomes strictly governed by the inherent reaction rate of the catalyst. The RZ is responsive to bulk concentrations of H_2 and NO_2^- and Pd-loading and therefore can be manipulated by the adjustment of any of these parameters, which will change observed kinetics as conditions within the RZ vary. Figure 5 applies to specific observations from this study only, and further investigation is required to develop a full understanding of the effects of hydrogel conditions and species concentrations on concentration profile development under a variety of conditions.

Byproduct selectivity is a critical outcome in evaluating the efficacy of the catalytic treatment of contaminants in water, and it can be used to further characterize the CHM. For NO_2^-, NH_4^+ forms selectively when the H/N ratio at catalytic active sites is high.[58] As listed in Table 1 and shown in Figure 6, the NH_4^+ selectivity declined with increasing Pd-loading and increased with reaction time for all samples. The NH_4^+ selectivity increased with reaction time because the H/N ratio increased as N was depleted (Figure 6A). Selectivity can also be altered by pH changes during the reaction.[60] Due to the low initial NO_2^- concentrations and relatively low conversions (<30%), minimal pH shifts were observed ($\Delta pH < 1$). Presumably, at higher Pd-loadings where the overall N removal is greater for the same reaction time, a higher NH_4^+ selectivity should be observed. This effect was not observed though, even when considering the selectivity at the same NO_2^- removal for each loading (Figure 6B). This behavior indicates that the Pd-loading is the dominant driver of NH_4^+ selectivity in the CHM, which is consistent with previous observations using other types of supports.[27,59]

The effect of Pd-loading on NH_4^+ selectivity in the CHM is best explained by considering the RZ and is conceptualized in Figure 5.[42] For lower Pd-loadings with a thicker RZ, NO_2^- will migrate deeper into the hydrogel from the bulk solution and N concentrations will be lower near the lumen wall where H_2 concentrations are the highest. This phenomenon results in a higher average H/N ratio, which increases the propensity for NH_4^+ formation. Conversely, higher Pd-loadings with a thinner RZ will have a lower average H/N ratio throughout the RZ, resulting in a lower selectivity for NH_4^+.

3.4. Effect of H_2 Delivery Method and Mass Transport on the Activity and Selectivity of NO_2^- Hydrogenation. Two co-diffusional experimental scenarios were used to determine the effects of mass transport of H_2 and NO_2^- on the activity and byproduct selectivity of NO_2^- hydrogenation. First, using a CHM (0.6 mg Pd), H_2 was bubbled directly into the bulk solution, similar to a traditionally supported catalyst. Then, the Pd nanoparticles (0.60 mg) were extracted from the CHM and the experiment was run again with H_2 bubbling directly into the bulk solution. This setup is similar to a traditional batch reactor with a suspended catalyst and was used to determine the effects of immobilizing the Pd within the CHM, by presumably eliminating mass transfer limitations caused by hydrogel film-diffusion.

The normalized first-order rate constants (k') for the counter-diffusional CHM, co-diffusional CHM, and co-diffusional suspension were 0.130, 0.168, and 0.180 L mol-Pd^{-1} s^{-1}, respectively. From these results, an activity ratio was calculated to highlight mass transfer limitations by the hydrogel and co-diffusional H_2 delivery. The activity ratio is defined herein as the ratio between the reaction rate of the supported catalysts to the suspended catalysts (e.g., counter-diffusional/suspended). The activity ratios were calculated to be 0.72 and 0.93 for counter-diffusion and co-diffusion systems, respectively. These results indicate that diffusion played a role in limiting the reaction rate. Furthermore, mass transport limitations in the co-diffusional system were lower compared to those in the counter-diffusional system, which is contrary to the premise that the counter-diffusional system should be more efficient. This outcome can be explained by considering the influence of hydrogel thickness on the counter-diffusion system. For the reaction to occur in the counter-diffusion system, the species must penetrate the hydrogel thickness to reach the RZ where both are present to react, while in the co-diffusion system, both species only diffuse as far as necessary to reach unfilled active sites.

For comparison, an additional experiment was conducted using a more densely loaded CHM (2.51 mg Pd). Similarly, the rate of the suspended catalysts (0.114 L mol-Pd^{-1} s^{-1}) was greater than those in the counter-diffusional system (0.062 L mol-Pd^{-1} s^{-1}), resulting in a comparatively lower activity ratio of 0.54. These results further confirm that the Pd mass-normalized activity of densely loaded CHMs is more significantly affected by diffusion limitations as the shallow RZ uses a lower percentage of Pd, and H_2 must diffuse further into the hydrogel from the HFM. Thus, to reduce mass transfer limitations in the counter-diffusional system, the thickness of the hydrogel and the Pd loading must be optimized.

DOI: 10.1021/acs.est.9b01667
Environ. Sci. Technol. XXXX, XXX, XXX−XXX

Although optimization of the counter-diffusional system to account for H_2 mass transfer limitations will be challenging, counter-diffusional systems are more efficient than co-diffusional systems because of the reduced H_2 consumption. Assuming that the H_2 consumption in the counter-diffusional system is driven by the reaction with NO_2^- and $O_{2(aq)}$, the total H_2 consumption during a 6 h hydrogenation experiment is estimated to be approximately 5.6−7.0 × 10^{-4} moles (see SI for calculation). For the co-diffusional and suspended catalysts systems, H_2 is bubbled into the bulk solution. This H_2 largely dissipates into the atmosphere, and the total consumption during a 6 h period, at a flow rate of 100 mL/min, is 1.47 mol, which is approximately four-orders of magnitude greater than that in the counter-diffusional system.

In this study, counter-diffusional experiments were conducted in closed-mode (i.e., where gas may only exit the lumen by diffusion through the wall), which greatly reduces overall H_2 consumption but encourages back-diffusion of inert gases (e.g., N_2) into the lumen. Back-diffusion lowers the overall H_2 availability and thus the activity. This inefficiency can be addressed by using simple operational modifications (e.g., periodic lumen venting) that can improve the activity of counter-diffusional reactors while preserving the advantages of closed-mode counter-diffusional reactors, including operational safety.[40]

Another benefit of the counter-diffusional system is the ability to control the amount of H_2 that reaches the RZ. For NO_2^- hydrogenation, a change in the H/N ratio at reactive sites greatly affects the byproduct selectivity. For, approximately, 25% NO_2^- removal, the NH_4^+ selectivity was 42%, 77%, and 92% for counter-diffusional, co-diffusional, and suspended catalyst systems, respectively. The supply of H_2 through the lumen allows control of the amount that reaches RZ since H_2 must diffuse through the hydrogel toward the bulk solution. Compared to the co-diffusional systems, the counter-diffusional system resulted in a lower H/N ratio and thus a lower NH_4^+ selectivity, in agreement with studies on the effect of the H_2 partial pressure.[42]

3.5. Short-Term Stability in Groundwater. To evaluate the potential of the CHM to operate under more realistic treatment conditions, hydrogenation of NO_2^- in groundwater was investigated for 3 days using a completely mixed flow reactor (Figure S2). The reactor consisted of eight CHMs in parallel to increase the overall Pd-loading in the system (10.42 mg), while maintaining a consistent Pd-loading for each CHM (1.30 ± 0.32 mg). Steady removal of NO_2^- occurred over the time period (Figure 7), indicating the short-term stability of the CHM. The overall percent removal of NO_2^- was 30% after 1 day, 31% after 2 days, and 29% after 3 days. The rate constant for NO_2^- was determined to be 0.073 L mol-Pd^{-1} s^{-1}, which is approximately the same for a similar Pd-loading in the single-fiber CHM and batch-recycle system (i.e., Table 1). Selectivity for NH_4^+ was found to be higher in the tested system, with the selectivity averaging 65% upon reaching steady state. The cause of this shift is unclear and will require further analysis of the effects of the individual components on the function of the catalytic hydrogels. These results confirm the intermediate time-scale stability of the CHM for drinking water treatment and suggest that further investigations into the long-term performance under other realistic water conditions are necessary (e.g., month-long tests, effect of biofilms, presence of sulfite).

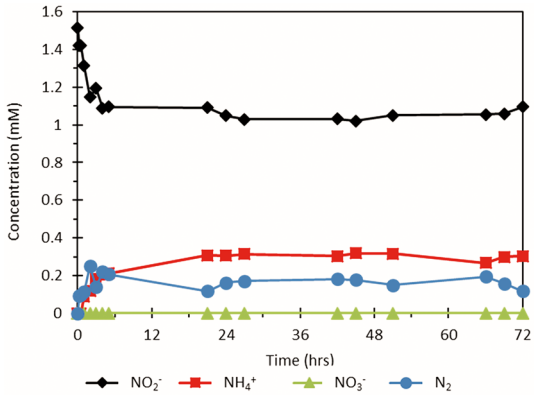

Figure 7. Conversion of NO_2^- in a groundwater in a continuous mixed flow reactor operated for 3 days. The reactor consisted of eight CHMs bundled together.

3.6. Comparison to Similar Systems and Future Directions. Results presented herein suggest that the CHM reactor is a promising new approach for the treatment of contaminants using HHCs. The fastest rates reported in this study for NO_2^- (Table S3; first-order k' = 0.213 L mol Pd^{-1} s^{-1}, zero-order k' = 5.41 mol-N mol-Pd^{-1}s^{-1} × 10^{-5}) are lower than the published rates for Pd on various supports in batch and continuous-flow reactors (Table S4), but direct comparisons are challenging due to the numerous operational differences (e.g., flow, pH, reactant concentration). The small difference in catalytic activity between the immobilized counter-diffusional operation and the suspended batch operation (activity ratio 0.54−0.72) further compares favorably to other immobilized systems, where greater reductions in activity have been reported by particle immobilization. Fiber-welded Pd−In nanoparticles showed lower activity by 3−4 times for NO_3^- removal compared to suspended particles,[34] while Pd−In catalysts operating in packed bed reactors showed a maximum activity that was 18% of what was observed during suspended batch operation.[19] Compared to a similar HFM reactor that used an alumina/carbon nanofiber membrane support for Pd (zero-order k' = 0.278 × 10^{-5} to 0.972 × 10^{-5} mol-N mol-Pd^{-1} s^{-1}),[42] the zero-order k' of the CHM was in a similar range despite the thicker support layer (2.22 to 5.41 × 10^{-5} mol-N mol-Pd^{-1} s^{-1}). This similarity suggests that the aqueous nature of the hydrogel promotes more rapid diffusion compared to the alumina support. However, even these results cannot be definitively compared due to differences in the reactor operation. In the batch-recycle reactor used with the CHM, a higher liquid velocity (1 cm s^{-1}) and initial NO_2^- concentration (0.35 mM) were used compared to the continuous-flow configuration of the alumina support (≈0.08 cm s^{-1}, 0.044 mM NO_2^-).[42] These conditions used with the CHM would minimize the development of stagnant layers and diffusion limitations in the system, thus increasing the overall reaction rate.

The low activity of the CHM can be improved through further testing and design optimization. While there are inherent challenges with respect to H_2 diffusion in the CHM due to the diffusive transport of H_2 to the catalysts, our results show that the use of a lower catalyst density reduces mass transport limitations. Optimization of the hydrogel (e.g., synthesis of more uniform, thinner hydrogel coatings) and the HFM (e.g., smaller diameter, thinner walls) can further improve mass transport. A significant limitation may be the

DOI: 10.1021/acs.est.9b01667
Environ. Sci. Technol. XXXX, XXX, XXX−XXX

inherent activity of the Pd catalyst itself, which was synthesized in situ in the CHM. Optimization of the synthesis procedure and the use of more active catalysts would greatly improve the overall reaction rate. One possibility is to use preformed nanoparticle catalysts that are mixed into the gel during synthesis, which is a promising direction for future studies. Finally, the hydrogenation of NO_2^- is dependent upon pH, and thus adding a buffer to the system (e.g., bubbling CO_2) can result in improved activities.

■ ASSOCIATED CONTENT

Supporting Information

The Supporting Information is available free of charge on the ACS Publications website at DOI: 10.1021/acs.est.9b01667.

Additional details on reactor configuration and experimental methods, water quality parameters for the model groundwater, SAED patterns for recovered Pd nanoparticles, H_2 and O_2 concentration profiles measured within the hydrogel without reaction, calculations for the estimated effective diffusivity and H_2 consumption, and a comparison of measured rates for this experiment and similar studies. (PDF)

■ AUTHOR INFORMATION

Corresponding Author

*Phone: 574-631-0305. E-mail: kdoudrick@nd.edu.

ORCID

Kyle Doudrick: 0000-0003-1912-9819

Notes

The authors declare no competing financial interest.

■ ACKNOWLEDGMENTS

This material is based upon work supported by the National Science Foundation under grant no. CBET-1847466.Additional support for Randal Marks came from the CEST/Bayer Predoctoral Research Fellowship [Center for Environmental Science and Technology at Notre Dame (CEST)] and the Patrick and Jana Eilers Graduate Student Fellowship for Energy Related Research [Center for Sustainable Energy at Notre Dame (ND Energy)]. The authors thank Dr. Sergei Rouvimov of the Notre Dame Integrated Imaging Facility for assistance with TEM and SAED analysis. The authors further thank CEST for access to instrumentation, including the IC, ICP, and microwave digester.

■ REFERENCES

(1) Soares, O. S. G. P.; Orfao, J. J. M.; Pereira, M. F. R. Activated Carbon Supported Metal Catalysts for Nitrate and Nitrite Reduction in Water. *Catal. Lett.* **2008**, *126* (3−4), 253−260.

(2) Prusse, U.; Vorlop, K. D. Supported bimetallic palladium catalysts for water-phase nitrate reduction. *J. Mol. Catal. A: Chem.* **2001**, *173* (1−2), 313−328.

(3) Shuai, D. M.; McCalman, D. C.; Choe, J. K.; Shapley, J. R.; Schneider, W. F.; Werth, C. J. Structure Sensitivity Study of Waterborne Contaminant Hydrogenation Using Shape- and Size-Controlled Pd Nanoparticles. *ACS Catal.* **2013**, *3* (3), 453−463.

(4) Chaplin, B. P.; Reinhard, M.; Schneider, W. F.; Schuth, C.; Shapley, J. R.; Strathmann, T. J.; Werth, C. J. Critical Review of Pd-Based Catalytic Treatment of Priority Contaminants in Water. *Environ. Sci. Technol.* **2012**, *46* (7), 3655−3670.

(5) Pintar, A.; Batista, J.; Levec, J.; Kajiuchi, T. Kinetics of the catalytic liquid-phase hydrogenation of aqueous nitrate solutions. *Appl. Catal., B* **1996**, *11* (1), 81−98.

(6) Yoshinaga, Y.; Akita, T.; Mikami, I.; Okuhara, T. Hydrogenation of nitrate in water to nitrogen over Pd-Cu supported on active carbon. *J. Catal.* **2002**, *207* (1), 37−45.

(7) Barrabes, N.; Sa, J. Catalytic nitrate removal from water, past, present and future perspectives. *Appl. Catal., B* **2011**, *104* (1−2), 1−5.

(8) Hu, M. C.; Liu, Y.; Yao, Z. H.; Ma, L. P.; Wang, X. Q. Catalytic reduction for water treatment. *Front. Environ. Sci. Eng.* **2018**, *12* (1), 9720 DOI: 10.1007/s11783-017-0972-0.

(9) Benck, J. D.; Hellstern, T. R.; Kibsgaard, J.; Chakthranont, P.; Jaramillo, T. F. Catalyzing the Hydrogen Evolution Reaction (HER) with Molybdenum Sulfide Nanomaterials. *ACS Catal.* **2014**, *4* (11), 3957−3971.

(10) Wang, Z. Y.; von dem Bussche, A.; Qiu, Y.; Valentin, T. M.; Gion, K.; Kane, A. B.; Hurt, R. H. Chemical Dissolution Pathways of MoS2 Nanosheets in Biological and Environmental Media. *Environ. Sci. Technol.* **2016**, *50* (13), 7208−7217.

(11) Sun, M.; Liu, H. J.; Qu, J. H.; Li, J. H. Earth-Rich Transition Metal Phosphide for Energy Conversion and Storage. *Adv. Energy Mater.* **2016**, *6* (13), 34.

(12) Chen, X.; Huo, X. C.; Liu, J. Y.; Wang, Y.; Werth, C. J.; Strathmann, T. J. Exploring beyond palladium: Catalytic reduction of aqueous oxyanion pollutants with alternative platinum group metals and new mechanistic implications. *Chem. Eng. J.* **2017**, *313*, 745−752.

(13) Choe, J. K.; Bergquist, A. M.; Jeong, S.; Guest, J. S.; Werth, C. J.; Strathmann, T. J. Performance and life cycle environmental benefits of recycling spent ion exchange brines by catalytic treatment of nitrate. *Water Res.* **2015**, *80*, 267−280.

(14) Davie, M. G.; Cheng, H. F.; Hopkins, G. D.; Lebron, C. A.; Reinhard, M. Implementing Heterogeneous Catalytic Dechlorination Technology for Remediating TCE-Contaminated Groundwater. *Environ. Sci. Technol.* **2008**, *42* (23), 8908−8915.

(15) Heck, K. N.; Garcia-Segura, S.; Westerhoff, P.; Wong, M. S. Catalytic Converters for Water Treatment. *Acc. Chem. Res.* **2019**, *52* (4), 906−915.

(16) Bergquist, A. M.; Bertoch, M.; Gildert, G.; Strathmann, T. J.; Werth, C. J. Catalytic Denitrification in a Trickle Bed Reactor: Ion Exchange Waste Brine Treatment. *Journal American Water Works Association* **2017**, *109* (5), E129−E143.

(17) Prusse, U.; Hahnlein, M.; Daum, J.; Vorlop, K. D. Improving the catalytic nitrate reduction. *Catal. Today* **2000**, *55* (1−2), 79−90.

(18) Bergquist, A. M.; Choe, J. K.; Strathmann, T. J.; Werth, C. J. Evaluation of a hybrid ion exchange-catalyst treatment technology for nitrate removal from drinking water. *Water Res.* **2016**, *96*, 177−187.

(19) Bertoch, M.; Bergquist, A. M.; Gildert, G.; Strathmann, T. J.; Werth, C. J. Catalytic Nitrate Removal in a Trickle Bed Reactor: Direct Drinking Water Treatment. *Journal American Water Works Association* **2017**, *109* (5), E144−E157.

(20) Calvo, L.; Gilarranz, M. A.; Casas, J. A.; Mohedano, A. F.; Rodriguez, J. J. Denitrification of Water with Activated Carbon-Supported Metallic Catalysts. *Ind. Eng. Chem. Res.* **2010**, *49* (12), 5603−5609.

(21) Pintar, A.; Batista, J. Catalytic hydrogenation of aqueous nitrate solutions in fixed-bed reactors. *Catal. Today* **1999**, *53* (1), 35−50.

(22) Horold, S.; Tacke, T.; Vorlop, K. D. CATALYTICAL REMOVAL OF NITRATE AND NITRITE FROM DRINKING-WATER. 1. SCREENING FOR HYDROGENATION CATALYSTS AND INFLUENCE OF REACTION CONDITIONS ON ACTIVITY AND SELECTIVITY. *Environ. Technol.* **1993**, *14* (10), 931−939.

(23) Horold, S.; Vorlop, K. D.; Tacke, T.; Sell, M. DEVELOPMENT OF CATALYSTS FOR A SELECTIVE NITRATE AND NITRITE REMOVAL FROM DRINKING-WATER. *Catal. Today* **1993**, *17* (1−2), 21−30.

(24) Vorlop, K. D.; Tacke, T. 1ST STEPS TOWARDS NOBLE-METAL CATALYZED REMOVAL OF NITRATE AND NITRITE FROM DRINKING-WATER. *Chem. Ing. Tech.* **1989**, *61* (10), 836−837.

(25) Matatov-Meytal, Y.; Barelko, V.; Yuranov, I.; Sheintuch, M. Cloth catalysts in water denitrification - I. Pd on glass fibers. *Appl. Catal., B* **2000**, *27* (2), 127−135.

(26) Matatov-Meytal, Y.; Barelko, V.; Yuranov, I.; Kiwi-Minsker, L.; Renken, A.; Sheintuch, M. Cloth catalysts for water denitrification II. Removal of nitrates using Pd-Cu supported on glass fibers. *Appl. Catal., B* **2001**, *31* (4), 233−240.
(27) Matatov-Meytal, Y.; Shindler, Y.; Sheintuch, M. Cloth catalysts in water denitrification - III. pH inhibition of nitrite hydrogenation over Pd/ACC. *Appl. Catal., B* **2003**, *45* (2), 127−134.
(28) Matatov-Meytal, U.; Sheintuch, M. Activated carbon cloth-supported Pd-Cu catalyst: Application for continuous water denitrification. *Catal. Today* **2005**, *102*, 121−127.
(29) Matatov-Meytal, U.; Sheintuch, M. The relation between surface composition of Pd-Cu/ACC catalysts prepared by selective deposition and their denitrification behavior. *Catal. Commun.* **2009**, *10* (8), 1137−1141.
(30) Chinthaginjala, J. K.; Bitter, J. H.; Lefferts, L. Thin layer of carbon-nano-fibers (CNFs) as catalyst support for fast mass transfer in hydrogenation of nitrite. *Appl. Catal., A* **2010**, *383* (1−2), 24−32.
(31) Espinosa, R. B.; Lefferts, L. Ni in CNFs: Highly Active for Nitrite Hydrogenation. *ACS Catal.* **2016**, *6* (8), 5432−5440.
(32) Ludtke, K.; Peinemann, K. V.; Kasche, V.; Behling, R. D. Nitrate removal of drinking water by means of catalytically active membranes. *J. Membr. Sci.* **1998**, *151* (1), 3−11.
(33) Wehbe, N.; Guilhaume, N.; Fiaty, K.; Miachon, S.; Dalmon, J. A. Hydrogenation of nitrates in water using mesoporous membranes operated in a flow-through catalytic contactor. *Catal. Today* **2010**, *156* (3−4), 208−215.
(34) Durkin, D. P.; Ye, T.; Choi, J.; Livi, K. J. T.; De Long, H. C.; Trulove, P. C.; Fairbrother, D. H.; Haverhals, L. M.; Shuai, D. M. Sustainable and scalable natural fiber welded palladium-indium catalysts for nitrate reduction. *Appl. Catal., B* **2018**, *221*, 290−301.
(35) Irfan, M.; Glasnov, T. N.; Kappe, C. O. Heterogeneous Catalytic Hydrogenation Reactions in Continuous-Flow Reactors. *ChemSusChem* **2011**, *4* (3), 300−316.
(36) Dittmeyer, R.; Hollein, V.; Daub, K. Membrane reactors for hydrogenation and dehydrogenation processes based on supported palladium. *J. Mol. Catal. A: Chem.* **2001**, *173* (1−2), 135−184.
(37) Martin, K. J.; Nerenberg, R. The membrane biofilm reactor (MBfR) for water and wastewater treatment: Principles, applications, and recent developments. *Bioresour. Technol.* **2012**, *122*, 83−94.
(38) Ahmed, T.; Semmens, M. J.; Voss, M. A. Oxygen transfer characteristics of hollow-fiber, composite membranes. *Adv. Environ. Res.* **2004**, *8* (3−4), 637−646.
(39) Pankhania, M.; Stephenson, T.; Semmens, M. J.; Inst Chem, E. HOLLOW FIBRE BIOREACTOR FOR WASTEWATER TREATMENT USING BUBBLELESS MEMBRANE AERATION. *Water Res.* **1994**, *28*, 356−358.
(40) Perez-Calleja, P.; Aybar, M.; Picioreanu, C.; Esteban-Garcia, A. L.; Martin, K. J.; Nerenberg, R. Periodic venting of MABR lumen allows high removal rates and high gas-transfer efficiencies. *Water Res.* **2017**, *121*, 349−360.
(41) Espinosa, R. B.; Rafieian, D.; Lammertink, R. G. H.; Lefferts, L. Carbon nano-fiber based membrane reactor for selective nitrite hydrogenation. *Catal. Today* **2016**, *273*, 50−61.
(42) Espinosa, R. B.; Rafieian, D.; Postma, R. S.; Lammertink, R. G. H.; Lefferts, L. Egg-shell membrane reactors for nitrite hydrogenation: Manipulating kinetics and selectivity. *Appl. Catal., B* **2018**, *224*, 276−282.
(43) Strukul, G.; Gavagnin, R.; Pinna, F.; Modaferri, E.; Perathoner, S.; Centi, G.; Marella, M.; Tomaselli, M. Use of palladium based catalysts in the hydrogenation of nitrates in drinking water: from powders to membranes. *Catal. Today* **2000**, *55* (1−2), 139−149.
(44) Saha, S.; Pal, A.; Kundu, S.; Basu, S.; Pal, T. Photochemical Green Synthesis of Calcium-Alginate-Stabilized Ag and Au Nanoparticles and Their Catalytic Application to 4-Nitrophenol Reduction. *Langmuir* **2010**, *26* (4), 2885−2893.
(45) Li, Y.; Li, G.; Li, W.; Yang, F.; Liu, H. H. Greenly Synthesized Gold-Alginate Nanocomposites Catalyst for Reducing Decoloration of Azo-Dyes. *Nano* **2015**, *10* (8), 1550108.
(46) Thangaraj, V.; Mahmud, S.; Li, W.; Yang, F.; Liu, H. H. Greenly synthesised silver-alginate nanocomposites for degrading dyes and bacteria. *IET Nanobiotechnol.* **2018**, *12* (1), 47−51.
(47) Ai, L. H.; Yue, H. T.; Jiang, J. Environmentally friendly light-driven synthesis of Ag nanoparticles in situ grown on magnetically separable biohydrogels as highly active and recyclable catalysts for 4-nitrophenol reduction. *J. Mater. Chem.* **2012**, *22* (44), 23447−23453.
(48) Ai, L. H.; Jiang, J. Catalytic reduction of 4-nitrophenol by silver nanoparticles stabilized on environmentally benign macroscopic biopolymer hydrogel. *Bioresour. Technol.* **2013**, *132*, 374−377.
(49) Chen, P.; Zhang, X. G.; Mia, Z. J.; Han, B. X.; An, G. M.; Liu, Z. M. In-Situ Synthesis of Noble Metal Nanoparticles in Alginate Solution and Their Application in Catalysis. *J. Nanosci. Nanotechnol.* **2009**, *9* (4), 2628−2633.
(50) Chtchigrovsky, M.; Lin, Y.; Ouchaou, K.; Chaumontet, M.; Robitzer, M.; Quignard, F.; Taran, F. Dramatic Effect of the Gelling Cation on the Catalytic Performances of Alginate-Supported Palladium Nanoparticles for the Suzuki-Miyaura Reaction. *Chem. Mater.* **2012**, *24* (8), 1505−1510.
(51) Lee, K. Y.; Mooney, D. J. Alginate: Properties and biomedical applications. *Prog. Polym. Sci.* **2012**, *37* (1), 106−126.
(52) Garbayo, I.; Leon, R.; Vigara, J.; Vilchez, C. Diffusion characteristics of nitrate and glycerol in alginate. *Colloids Surf., B* **2002**, *25* (1), 1−9.
(53) Sonderholm, M.; Kragh, K. N.; Koren, K.; Jakobsen, T. H.; Darch, S. E.; Alhede, M.; Jensen, P. O.; Whiteley, M.; Kuhl, M.; Bjarnsholt, T. Pseudomonas aeruginosa Aggregate Formation in an Alginate Bead Model System Exhibits In Vivo-Like Characteristics. *Appl. Environ. Microbiol.* **2017**, *83* (9), No. e00113.
(54) Choudhary, V. R.; Samanta, C.; Choudhary, T. V. Direct oxidation of H_2 to H_2O_2 over Pd-based catalysts: Influence of oxidation state, support and metal additives. *Appl. Catal., A* **2006**, *308*, 128−133.
(55) Matsis, V. M.; Grigoropoulou, H. P. Kinetics and equilibrium of dissolved oxygen adsorption on activated carbon. *Chem. Eng. Sci.* **2008**, *63* (3), 609−621.
(56) Pintar, A.; Bercic, G.; Levec, J. Catalytic liquid-phase nitrite reduction: Kinetics and catalyst deactivation. *AIChE J.* **1998**, *44* (10), 2280−2292.
(57) Ebbesen, S. D.; Mojet, B. L.; Lefferts, L. In situ ATR-IR study of nitrite hydrogenation over Pd/Al_2O_3. *J. Catal.* **2008**, *256* (1), 15−23.
(58) Shin, H.; Jung, S.; Bae, S.; Lee, W.; Kim, H. Nitrite Reduction Mechanism on a Pd Surface. *Environ. Sci. Technol.* **2014**, *48* (21), 12768−12774.
(59) Holler, V.; Radevik, K.; Yuranov, I.; Kiwi-Minsker, L.; Renken, A. Reduction of nitrite-ions in water over Pd-supported on structured fibrous materials. *Appl. Catal., B* **2001**, *32* (3), 143−150.
(60) Ebbesen, S. D.; Mojet, B. L.; Lefferts, L. Effect of pH on the Nitrite Hydrogenation Mechanism over Pd/Al_2O_3 and Pt/Al_2O_3: Details Obtained with ATR-IR Spectroscopy. *J. Phys. Chem. C* **2011**, *115* (4), 1186−1194.

DOI: 10.1021/acs.est.9b01667
Environ. Sci. Technol. XXXX, XXX, XXX−XXX